ORIGINAL ARTICLE

Adaptive Optics Scanning Laser Ophthalmoscope-Based Microperimetry

William S. Tuten*, Pavan Tiruveedhula†, and Austin Roorda‡

ABSTRACT

Purpose. To develop and test the application of an adaptive optics scanning laser ophthalmoscope (AOSLO) with eye tracking for high-resolution microperimetric testing.

Methods. An AOSLO was used to conduct simultaneous high-resolution retinal imaging and visual function testing in six normal subjects. Visual sensitivity was measured at test locations between the fovea and 5.0° eccentricity via an increment threshold approach using a 40-trial, yes-no adaptive Bayesian staircase procedure (QUEST). A high-speed eye tracking algorithm enabled real-time video stabilization and the delivery of diffraction-limited Goldmann I-sized stimuli (diameter = 6.5 arc min = ~32 μm; λ = 680 nm) to targeted retinal loci for 200 ms. Test locations were selected either manually by the examiner or automatically using Fourier-based image registration. Cone spacing was assessed at each test location and sensitivity was plotted against retinal eccentricity. Finally, a 4.2 arc min stimulus was used to probe the angioscotoma associated with a blood vessel located at 2.5° eccentricity.

Results. Visual sensitivity decreases with eccentricity at a rate of −1.32 dB/deg (R^2 = 0.60). The vertical and horizontal errors of the targeted stimulus delivery algorithm averaged 0.81 and 0.89 arc min (~4 μm), respectively. Based on a predetermined exclusion criterion, the stimulus was successfully delivered to its targeted location in 90.1% of all trials. Automated recovery of test locations afforded the repeat testing of the same set of cones over a period of 3 months. Thresholds measured over a parafoveal blood vessel were 1.96 times higher (p < 0.05; one-tailed t-test) than those measured in directly adjacent retina.

Conclusions. AOSLO-based microperimetry has the potential to test visual sensitivity with fine retinotopic precision. Automated recovery of previously tested locations allows these measures to be tracked longitudinally. This approach can be implemented by researchers interested in establishing the functional correlates of photoreceptor mosaic structure in patients with retinal disease.

(Optom Vis Sci 2012;89:563–574)

Key Words: adaptive optics, microperimetry, scanning laser ophthalmoscopy

The introduction of adaptive optics (AO) into ophthalmic imaging systems by Liang et al.[1] in 1997 ushered in a new frontier in retinal imaging. By measuring and compensating for the high-order monochromatic aberrations of the eye, it became possible to collect images of the living retina in which individual photoreceptor cells could be reliably resolved. While the earliest forays into AO-based imaging primarily dealt with describing the normal cone photoreceptor mosaic,[1–3] one immediately obvious application of high-resolution retinal imaging is in its potential to observe and characterize the structural changes associated with retinal disease on the cellular scale.

The adaptive optics scanning laser ophthalmoscope (AOSLO) is one such AO-based imaging modality,[4] and it has been used extensively to characterize the cone photoreceptor mosaic in both normal subjects and patients with retinal disease.[5–10] Over the past 10 years, AOSLO imaging systems have continued to evolve. Increasingly finer structures, including rod photoreceptors and foveal cones, are now resolvable.[11–13] A recent investigation in a group of patients with retinitis pigmentosa demonstrated that cone mosaic structure can be followed longitudinally in a patient population, suggesting that AOSLO imaging may be an especially sensitive outcome measure for clinical trials evaluating treatments aimed to slow down the progression of retinal disease.[8]

*OD, MS
†MS
‡PhD
School of Optometry, University of California, Berkeley, Berkeley, California.

While AOSLO can be used to track high-resolution structure in the retina over time, the functional consequences of subtle changes in the photoreceptor mosaic are difficult to elucidate. In patients with retinal disease, AOSLO images often contain patches where photoreceptor structure is ambiguous, owing to an increased presence of factors that compromise imaging, such as media opacities, retinal edema, and weakly reflecting cones. To ensure that high-fidelity metrics of photoreceptor distribution (i.e., cone spacing and cone density) can be obtained in this population, it becomes necessary to select regions of interest (ROIs) within AOSLO images where unambiguous arrays of cones can be identified and tracked longitudinally. Often, these ROIs span relatively small patches of retina; for example, ROI width ranged between 0.2° and 0.6° in Ref. 8.

If AOSLO imaging is to emerge as an objective marker of disease progression, the notion that a visible cone is a functional cone must be tested. To best accomplish this, the functional status of the cones located within these small ROIs needs to be established with confidence. In addition to describing the function of cones that can be easily resolved, tools capable of such high-precision visual function testing would also deepen our understanding of the regions in AOSLO images where photoreceptor mosaic structure is ambiguous or compromised.

Unfortunately, correlating structural findings from AOSLO imaging with results from conventional perimetric devices is prone to imprecision. These traditional instruments offer a limited array of test patterns and are unable to monitor and correct for small fixational eye movements, leaving the examiner to infer which regions of the retina were stimulated during a given visual field test and unable to target specific ROIs for functional assessment.

Fundus-related perimetry, often referred to as microperimetry, obviates this need for inference by conducting simultaneous retinal imaging and visual function testing, allowing more precise structure-function correlations to be established in patients with retinal disease.[14–17] While custom-built and commercially available microperimeters may feature some form of eye tracking, which allows the delivery of stimuli to targeted locations,[18,19] their ability to target and test visual function in regions as small as the ROIs delineated in AOSLO images is less than ideal. For instance, in a commercially available microperimeter (MP1, Nidek Technologies, Padua, Italy), a mean eye tracking accuracy of 4.9 arc min has been reported,[20] and the image registration between the infrared (IR) tracking image and color fundus photograph on which results are plotted is subject to errors as large as 2°.[21,22] Given that the smallest stimulus presented by the MP1 is Goldmann I-sized (6.5 arc min diameter), this system may lack the precision to probe visual function over time within a retinal region as small as 12×12 arc min.

To put the high-resolution structural data obtained with AOSLO imaging into a more meaningful context, tools capable of testing visual function on a commensurate scale are needed. One solution to this problem is to add microperimetry capabilities to the AOSLO system. In this study, we describe a method to quickly and efficiently conduct measures of visual sensitivity using diffraction-limited stimuli delivered to targeted retinal regions with single cone precision.[23,24] Although many of the features that distinguish AOSLO-based microperimetry from other perimetric devices have already been applied to the study of primate electrophysiology,[25] here we present a more efficient and robust system that can be used in humans—in both normal subjects and patients with retinal disease—to image and test a region of cones simultaneously, with the capacity to follow these measures longitudinally. Ultimately, this method has the potential to define structure-function relationships in the human retina on the cellular scale, and it may allow the functional consequences of photoreceptor loss—both diffuse and focal—to be established with increased confidence.

METHODS

Participants

Six normal subjects were recruited from the student and faculty population of the University of California, Berkeley. Before enrollment, informed consent was obtained after the study protocol and its potential risks and complications were presented to the subject in verbal and written form. The study design and informed consent documents were approved by the University of California Institutional Review Board, and the research was conducted in accordance with the tenets of the Declaration of Helsinki. The participants were five males and one female, with an average age of 32.5 years (SD = 7.3; range = 25 to 44).

Measuring Visual Sensitivity Across Eccentricity

Simultaneous high-resolution retinal imaging and visual function testing were conducted using an AOSLO. The specifics of imaging and conducting psychophysical experiments with AOSLO have been described elsewhere.[4,12,26–28] For the purposes of this report, the general nature of the psychophysical task and the data analysis associated with measuring visual sensitivity using AOSLO will be described first, and the details of AOSLO imaging, stimulus generation and delivery, test location selection, and light source calibration will be discussed in the ensuing sections.

An increment threshold approach was used to measure visual sensitivity at various retinal eccentricities between 0° and 5° along the temporal horizontal meridian of one eye. For each eccentricity, thresholds were measured a total of eight times over the course of two testing sessions. The retinal loci targeted for sensitivity testing were either chosen manually by the observer (subjects 1 to 5) or using software designed to automatically recover previously tested locations (subject 6). The background for testing was produced by a 2.1° × 2.1° raster scan of the 840 nm imaging superluminescent diode (SLD; Superlum, Carrigtwohill, Ireland), and the test stimulus was generated by a 680 nm SLD (Superlum) controlled by an acousto-optic modulator (AOM; Brimrose Corporation, Baltimore, MD) operating at up to 50 MHz.[29] The retinal illuminance of the background was 1.97 log Trolands. The power of the stimulus light source is adjustable, and for the data presented in this study its maximum power was set to 26 nW, corresponding to a maximum retinal illuminance of 3.45 log Trolands for the Goldmann I-sized stimulus (diameter = 6.5 arc min; ~32 μm on the retina) used in this study. The AOSLO-based microperimetry protocol was implemented via a custom software interface used for programming psychophysical experiments in our laboratory (Matlab, Mathworks, Natick, MA). All data presented in this re-

port were collected using a self-paced 40-trial QUEST staircase with a yes-no response paradigm.[30]

To measure sensitivity, dynamic AO imaging was initiated (for details, see next section), allowing retinal videos to be stabilized against a reference frame in real-time and the region targeted for stimulus delivery to be selected. A high-speed image-based eye tracking algorithm was used to track the retinal locus targeted for testing and generate a prediction on when to deliver the perimetric stimulus.[23,24] Each individual trial of the psychophysical staircase was initiated by the subject with a button push, triggering the recording of a 1 s imaging video during which the perimetric stimulus was delivered to the targeted retinal location non-continuously over a period of 200 ms. Poor image quality and fixational eye movements greater than ~50% of the raster size can both cause the image-based eye tracking algorithm to fail. When this was the case, stimulus delivery would not be initiated. To help differentiate between true negatives and trials during which stimulus delivery was not triggered, an auditory cue was provided for the subject whenever the voltage signal was sent to the AOM to deliver the stimulus. Individual trials during which stimulus delivery failed were immediately repeated. After stimulus presentation, the subject indicated their response via keyboard press and then initiated the next trial. Each response and its associated experimental parameters were saved to a text file for subsequent analysis.

Once all measures of visual sensitivity were collected, experiment videos were processed offline to generate retinal images with high signal-to-noise ratios. Because pixel position and time are coupled in raster-based imaging, a white digital cross corresponding to the center of the stimulus can be digitally written onto the video frame at the pixel location corresponding to when the AOM was triggered to deliver the stimulus, resulting in an unambiguous record of where the stimulus was delivered on the retina (see Video, Supplemental Digital Content 1, http://links.lww.com/OPX/A84, which demonstrates targeted stimulus delivery in AOSLO-based microperimetry). Stimulus delivery location was determined for each trial by locating the digital marker, allowing the removal of trials where delivery was spatially errant or failed entirely. Individual trials with a delivery error >4 pixels (~1.0 arc min) were excluded from analyses; when necessary, thresholds were recomputed using only trials where the stimulus fell within the inclusion window.

Next, the test location for each sensitivity measure was plotted onto an AOSLO image montage, and the distance to the subject's preferred retinal locus of fixation was calculated. An example of the test locations for AOSLO-based microperimetry is shown in Fig. 1. Measured visual thresholds ($T_{measured}$) were converted to sensitivities in decibels (S_{dB}) using Eq. 1, where T_{max} is the maximum retinal illuminance produced by the stimulus light source and $T_{measured}$ is the retinal illuminance at threshold, both in Trolands:

$$S_{dB} = 10 \times \log_{10}(T_{max}/T_{measured}) \qquad (1)$$

While expressing sensitivity in decibels is common in the perimetric literature, it should be cautioned that this scale simply reflects the ratio of the threshold retinal illuminance to the maximum retinal illuminance the perimeter is capable of displaying. Because these basic parameters differ from device to device, sensitivities in decibel values are not directly comparable across instruments. For these reasons, all data presented in this report include both the decibel scale specific to AOSLO-based microperimetry and the corresponding threshold value in log Trolands.

Visual sensitivities were plotted as a function of retinal eccentricity, and a linear regression was fit to the data using curve fitting software (Matlab, Mathworks). Cone photoreceptors were identified in the AOSLO images using a combination of manual and automated cone counting software, allowing metrics of photoreceptor distribution to be calculated.[31] Cone spacing data were used to estimate the number of cones sampling the perimetric stimulus. To ensure high-fidelity cone spacing data, only test locations beyond 2° retinal eccentricity were included in this analysis. Visual sensitivity was plotted as a function of the number of cones sampling the stimulus and a linear regression was fit to the data.

High-Resolution Retinal Imaging with AOSLO

Twenty minutes before AOSLO imaging, one drop of 1% tropicamide and one drop of 2.5% phenylephrine are instilled to achieve mydriasis and cycloplegia. Once the pupil is sufficiently dilated, the subject is situated in a chin rest mounted on an X-Y-Z stage and the pupil is aligned with the imaging beam. Head stabilization is aided using padded temple mounts and subject fixation is guided using a laser-illuminated spot on a screen external to the
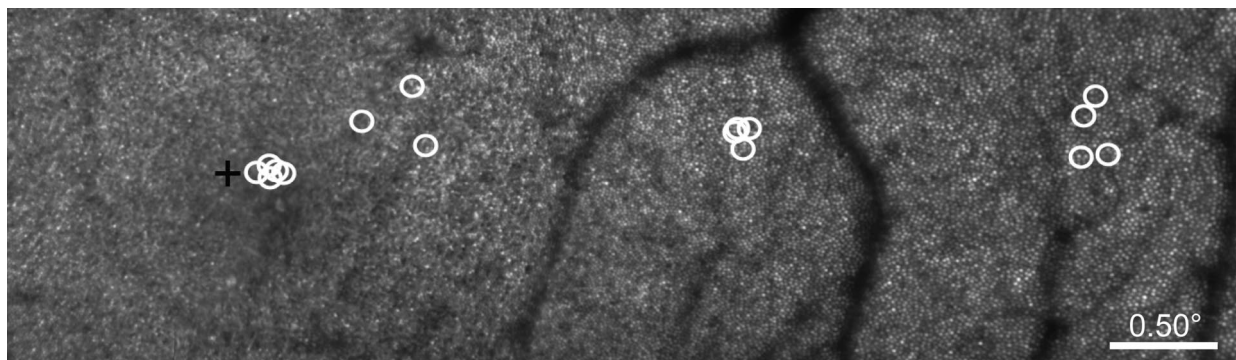
FIGURE 1.

Microperimetric testing locations for subject 3 plotted on an AOSLO-generated retinal image montage. Manually selected test locations for AOSLO-based microperimetry are denoted by the white circles, the size of which represents the size of the perimetric stimulus on the retina (Goldmann I = 6.5 arc min = ~32 μm). The subject's preferred retinal locus of fixation is marked by the black cross.

system. All wavefront sensing and correction are done over a 6 mm pupil.

To generate an image using an AOSLO, a focused spot from an 840 nm broadband superluminescent diode, or SLD, is scanned across the retina in a raster pattern using an analog-driven resonant scanner (Electro-Optics Products Corporation, Flushing Meadows, NY) in combination with a galvometric scanner (Cambridge Technology, Lexington, MA). A calibration grid placed at the retinal plane of a model eye is used to set the imaging field size and to compensate for the image distortions caused by the sinusoidal resonant scanner. In this study, raster scanning amplitudes were set so that each AOSLO image corresponded to approximately 2.1° × 2.1° (~630 × 630 μm) of retina. The light emerging from the eye is descanned by the scanning elements as it returns along the path of the beam, and the ocular monochromatic aberrations encoded therein are monitored with a custom-built Shack-Hartmann wavefront sensor and corrected dynamically with a 140 actuator, 5.5 μm stroke MEMS deformable mirror (Boston Micromachines, Cambridge, MA). Because the aberrometry beacon is scanned across the imaging field and the wavefront sensor samples at a maximum rate of 24 Hz, the measured wavefront represents a spatio-temporal average of the error for that patch of retina.

A photomultiplier tube (PMT; Hamamatsu, Japan) records the intensity of the reflected light, and pixel location is assigned using positional information from the scanning mirrors, allowing high-resolution retinal videos to be reconstructed over time by a frame grabber at a rate of 30 frames/s. Each frame comprises 512 × 512 pixels, which are digitized at rate of 20 MHz (pixel clock: 50 ns). Thus, for a 0.60° raster size, a single pixel corresponds to 4.21 arc sec (0.35 μm); for a 2.1° raster, a single pixel subtends 14.8 arc sec (1.23 μm; on the order of a foveal cone diameter[32]) of visual angle.

Light Source Calibration and Stimulus Delivery

The test stimulus is generated using a 680 nm SLD which is introduced into the light delivery arm of the AOSLO and is aligned to travel coincident to the imaging beam along the main optical path of the system. Because an IR light source is used for wavefront sensing and correction, the vergence of the stimulus light source as it enters the system must be adjusted to compensate for the roughly 0.5 D of longitudinal chromatic aberration (LCA).[13,33] The fidelity of LCA correction is confirmed by imaging the photoreceptor layer simultaneously with 680 and 840 nm light; when LCA is properly corrected, the photoreceptor mosaic is in sharp focus in both images.

The intensity of the stimulus light source is controlled by an analog-driven high-speed AOM, allowing custom stimulus patterns to be presented to the retina. The AOM works by diffracting the incoming light into multiple orders. Light scattered into the first-order diffraction mode is coupled into the AOSLO system. The magnitude of the diffracted power, and hence the luminance of the stimulus in the AOSLO, depends on the voltage used to drive the AOM. The voltage-response curve of the AOM used to control the stimulus luminance is non-linear. To generate a look-up table, a linear set of voltages from a 14-bit digital-to-analog converter is used to drive the AOM, and the radiant flux at the pupil plane is measured using an optical power meter (Newport

Corporation, Irvine, CA) at each step. While the digital-to-analog converter putatively offers 14-bit (=16,384 levels) modulation, the linearization process restricts this operational range; for this study, the stimulus intensity was modulated over a range of 1000 linearized steps (equivalent to a 30 dB range of modulation).

There are two important consequences to using an AOM to control our perimetric stimulus. The first is that some light will always scatter into the first-order direction, even when no voltage is sent to the AOM. The resulting leak must be measured to determine its contribution to the apparent luminance of the raster. When the stimulus light source was set to a maximum power of 26 nW, the AOM leak was on the order 0.2 nW (=1.29 log Trolands calculated for a field size of 4.41 deg²); however, as the power incident on the AOM is increased, the amount of light leaking through the AOM also increases, resulting in different background intensities at different power settings. Second, because the stimulus is generated pixel-by-pixel by the scanned laser, the actual amount of time the retina is exposed to the stimulus beam is a fraction of the nominal stimulus duration. The true stimulus duration is the sum of the number of pixels comprising the stimulus multiplied by the product of the number of frames over which the stimulus is presented and the time attributed to each pixel. Although the subject perceives the stimulus as continuous, this fact must be considered when calculating retinal illuminance.

Automated Retrieval of Previously Tested Locations

Due to normal fixational drift and the subtle intersession variations in raster scanning geometry that result from manually setting the field size, optimal real-time image stabilization is best achieved using a reference frame selected immediately before capturing a video. Therefore, each psychophysical procedure (i.e., a 40-trial staircase) is associated with a unique reference frame, and the x and y coordinates marking the retinal target in one reference frame will not necessarily correspond to the same retinal location in subsequent reference frames. Although stimulus delivery to a targeted retinal location during a given psychophysical procedure can achieve single cone precision, it is difficult when manually selecting test locations to consistently target the same patch of cones for repeat testing, especially near the fovea where there are fewer retinal landmarks (see Fig. 1).

To mitigate this problem, custom software was incorporated into the current imaging interface[24] to enable the automated retrieval of previously tested locations. When a given ROI is tested for the first time, the x and y coordinates of the location selected for targeted delivery are saved. At subsequent sessions, the original test location can be recalled by using a fast image registration algorithm[34] to calculate the shift between the original reference frame and the current reference frame. Applying this shift to the saved x and y coordinates of the original reference frame allows the original retinal test location to be identified and targeted in the x and y coordinates of the current reference frame. A schematic of this registration process is shown in Fig. 2.

Probing Angioscotomas

Finally, to further test the level of stimulus control offered by AOSLO-based microperimetry, the methods described in the pre-
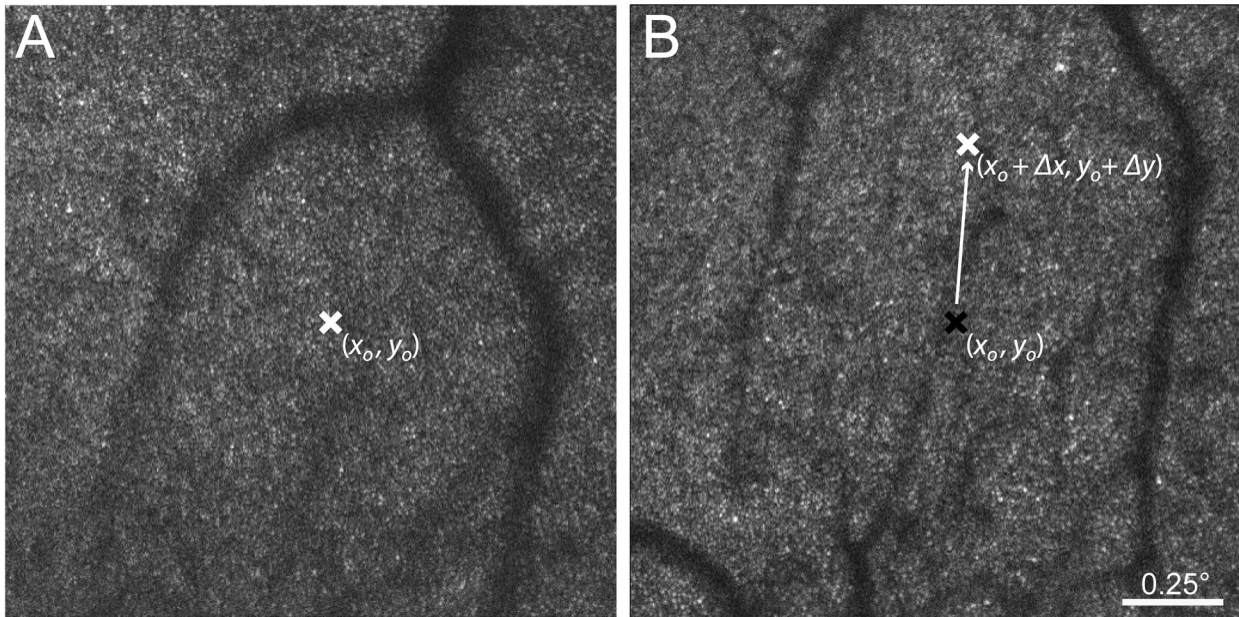
FIGURE 2.

Schematic illustrating automated retrieval of retinal loci previously tested with AOSLO-based microperimetry. (A) The reference frame for real-time video stabilization from a previous testing session with the retinal location (x_o, y_o) targeted for sensitivity testing indicated by the white "x." (B) The reference frame from a subsequent testing session. The reference frame in (B) is registered to the frame in (A), and the shift $(\Delta x, \Delta y)$ between the two images is applied to the target x and y coordinates of the original frame (black "x") to retrieve the previously tested retinal location (white "x") automatically.

ceding sections were used to measure visual thresholds in one subject on and around a parafoveal blood vessel (eccentricity = 2.5°) using a 4.2 arc min stimulus. Because the retinal vasculature is located anterior to the photoreceptor layer, the blood vessels cast a shadow on the underlying retina, resulting in a corresponding decrease in visual sensitivity known as angioscotoma.[35] Three measures of visual threshold were collected at each of three locations, including one directly over a blood vessel whose luminal diameter was roughly equal to the stimulus size (~21 μm). Measured sensitivities were averaged based on location and compared statistically using a two-tailed t-test. To test visual sensitivity over the blood vessel, it was necessary to increase the maximum power of the stimulus light source to 0.68 μW, which produced a maximum retinal illuminance of 4.85 log Trolands for a stimulus of this size. Because increasing the stimulus light source intensity results in an increased amount of light leaking through the AOM when it is switched off, the background retinal illuminance increased by roughly 50% for this power setting. Thus, the threshold values plotted in Figs. 5C and 6A should not be compared directly.

RESULTS

Stimulus Delivery and Automated Recovery of Tested Locations

The performance of real-time eye tracking, which allows for targeted stimulus delivery to selected retinal locations, is demonstrated in Fig. 3. When fixation was stable and photoreceptor mosaic structure was well resolved in the images, high-speed eye tracking and targeted stimulus delivery enabled the same patch of cones to be stimulated on 100% of trials; by contrast, without high-speed eye tracking, any given cone will be stimulated only on

a fraction of trials, even with good fixation. Across all test locations and subjects, the vertical and horizontal stimulus delivery errors averaged 0.81 and 0.89 arc min (~4 μm), respectively. On average, delivery errors were isotropic (p = 0.14, two-tailed t-test). In general, tracking performed best at test locations beyond 1° eccentricity, owing to retinal features becoming more easily resolved with increasing eccentricity. Based on our predetermined exclusion criterion, the stimulus was delivered to its targeted location in 90.1% of all trials.

Fig. 4 demonstrates the automated recovery of previously tested locations. Although the majority of the data presented in this study were collected at retinal loci manually selected by the examiner, the automated recovery allows AOSLO-based microperimetry testing to be repeated at the same retinal location with good precision. Stimulus location recovery appears robust to reference frame misalignments and can retrieve previously tested locations over a period of several months.

Measuring Visual Sensitivity with AOSLO-Based Microperimetry

Results from angioscotoma testing in subject 3 are shown in Fig. 5. Visual sensitivity for stimuli targeted at the retinal blood vessel is significantly lower than those measured in directly adjacent retina (Fig. 5C; p < 0.05, two-tailed t-test), indicating a relative angioscotoma. The relationship between visual sensitivity and retinal eccentricity is plotted in Fig. 6A; visual sensitivity as a function of the number of cones sampling the stimulus is shown in Fig. 6B. Visual sensitivity to the Goldmann I-sized stimulus decreases as a function of increasing eccentricity (Fig. 6A; slope = −1.32 dB/deg; R^2 = 0.60; p < 0.001). Beyond 2°, there is a significant
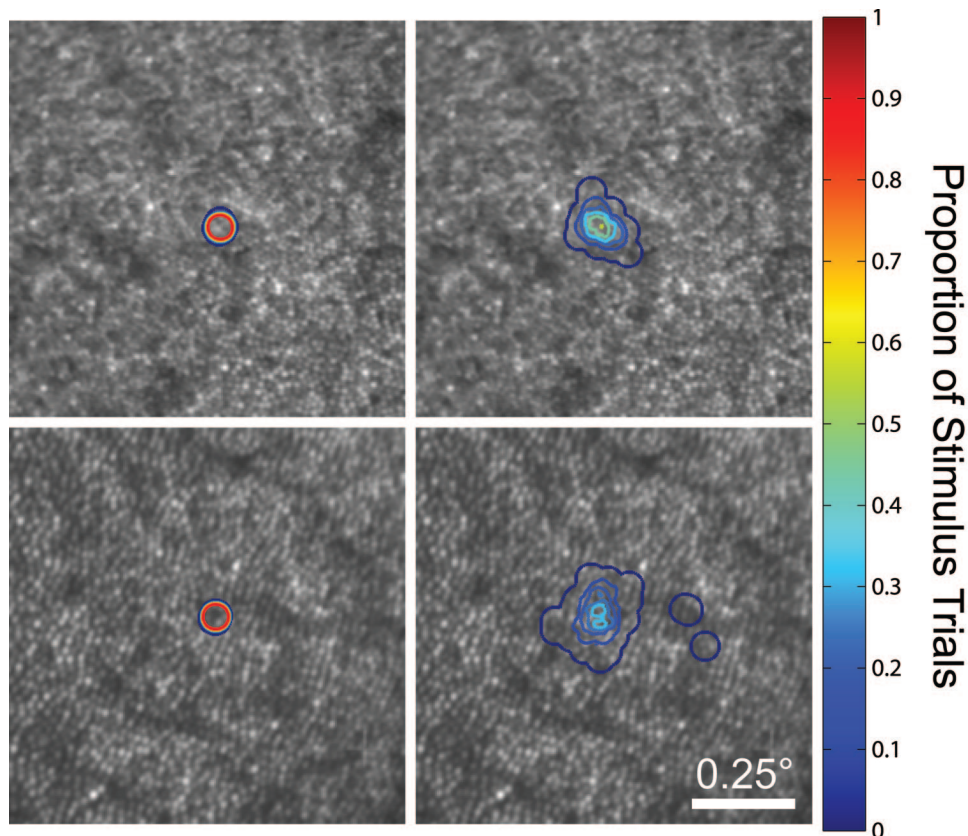
FIGURE 3.
Stimulus delivery contour plots for AOSLO-based microperimetry. Contour lines delineate the proportion of trials that a given pixel was stimulated during a psychophysical task (n = 60 trials). Stimulus delivery plots are shown for conditions with (left) and without (right) eye tracking at two eccentricities (top: 0.5°; bottom: 1.5°).

correlation between visual sensitivity and the number of cones sampling the perimetric stimulus, as estimated from cone spacing measures (Fig. 6B; slope = 0.19; R^2 = 0.41, p < 0.001).

DISCUSSION

Controlling the Perimetric Stimulus

The results of this study demonstrate that high precision visual function testing can be achieved with AOSLO-based microperimetry. With dynamic AO correction in place, stimuli that are at or near the diffraction limit can be presented to the subject's retina, leaving the examiner more confident about the pattern of light that is being sampled by the photoreceptors, as is shown in Fig. 7. Although monitoring and correcting high-order aberrations is not an infallible process, an advantage of conducting simultaneous retinal imaging and visual function testing—compared with a non-imaging AO psychophysics system—is that the sharpness of the perimetric stimulus in the imaging plane is directly tied to image quality, minimizing the need to rely on other metrics, such as root mean square deviation or Strehl ratio, as an indicator of stimulus fidelity. However, it bears mentioning that any stimulus—AO-corrected or not—is subject to scatter as it travels through the retina, and in confocal imaging systems, the degree of scatter in layers not conjugate with the imaging pinhole is not conveyed in the collected image.

Herein, we report values for cone-targeted stimulus delivery errors that are roughly three times higher than those previously reported using the same high-speed eye tracking algorithm.[23] The precision of image-based eye tracking and targeted stimulus delivery is primarily contingent on image quality and fixation stability. In both cases, the imaging field size plays a critical role. With regard to image quality, the use of an imaging field larger than the isoplanatic patch of the human eye—about 1°[36]—may result in images of suboptimal quality secondary to variations in the monochromatic aberrations as the wavefront sensor beacon is scanned across the retina. In addition, decreased spatial sampling is inherent to larger raster dimensions if the pixel clock remains fixed, further reducing image resolution. On the other hand, a larger imaging window allows more room for fixational instability, as any eye movement larger than ~50% of the imaging field can cause the ROI targeted for testing to move out of the imaging window, rendering the stimulus undeliverable. Thus, in patients with retinal disease whose fixation may be less stable than normal, the desire for obtaining the highest quality images may need to be balanced against the efficiency with which the AOSLO-based microperimetry system can deliver stimuli to targeted locations.

With this in mind, a 2.1° field size was chosen so that these results might be compared against future testing in patients with retinal disease. While the test conditions described in this report are not optimal for targeted stimulus delivery, a delivery error of
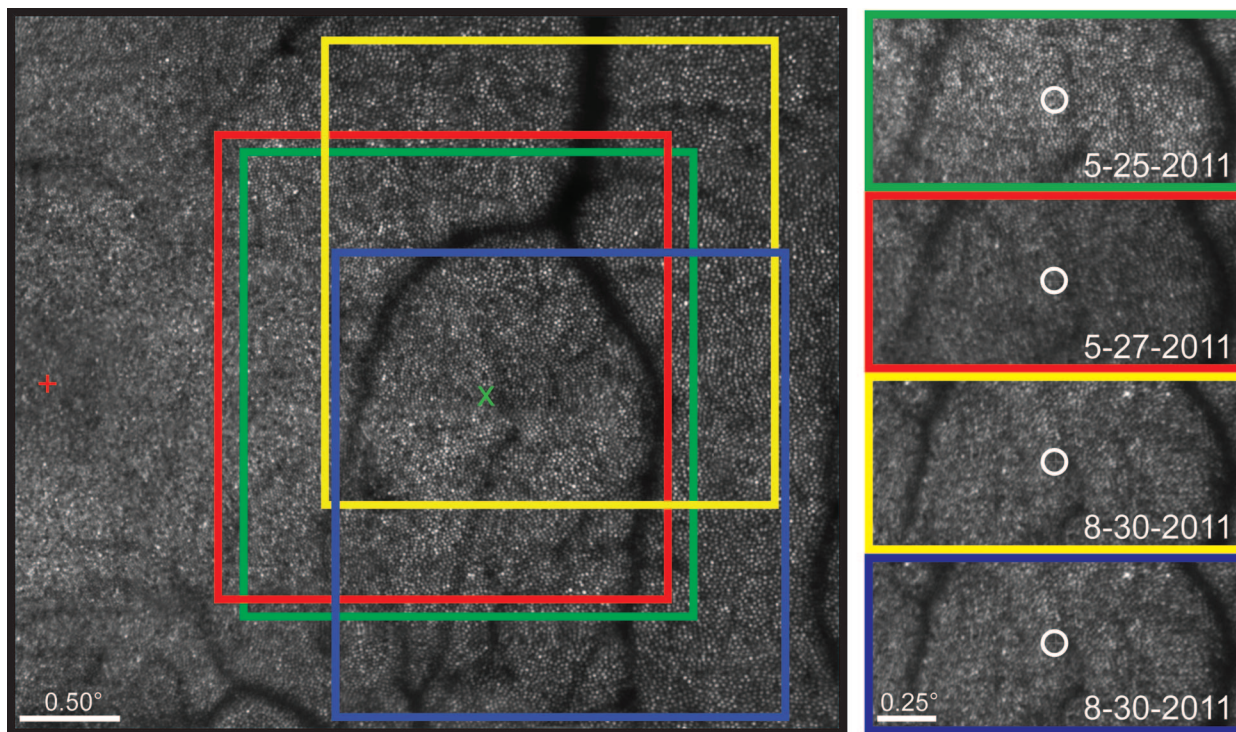
FIGURE 4.

Automated stimulus location recovery in subject 3. Left: Highlighted regions corresponding to individual reference frames used to collect stabilized retinal videos at ~2.5° retinal eccentricity. The original reference frame is outlined in green and the targeted retinal location for stimulus delivery is marked by the green "x." To retrieve the original test location, subsequent reference frames (red, yellow, blue) are registered against the original, and the shift is used to define the targeted retinal locus in the x-y coordinates of the new reference frame. The subject's preferred retinal locus of fixation is represented by the red cross. Right: The Goldmann I-sized white circles are plotted at the average stimulus delivery location for a 40-trial psychophysical task performed at baseline, baseline + 2 d, and baseline + 3 mo.

0.89 arc min is still less than the cone-to-cone spacing at all eccentricities beyond 1°[32] and is ~5.5× better than the tracking errors reported in the MP1.[20] In the end, the exclusion criterion for errant stimulus delivery can be relaxed or tightened during postprocessing, depending on the desired spatial resolution of the sensitivity measures.

Although the reflectance of single cones in the photoreceptor mosaic fluctuates over periods of minutes, and these fluctuations are independent between adjacent cones,[37] the Fourier-based stimulus location recovery software works over a period of at least 3 months in normal subjects. While the majority of the data presented in this report were collected before it was implemented, this software will enable measures of visual sensitivity at a specific retinal location to be repeated with confidence, allowing the function of a given patch of cones to be followed longitudinally. It is likely that this image registration algorithm is driven primarily by alignment of the cone mosaic. If true, this will serve to limit the precision of the registration in cases where there are disease-induced changes to the cone mosaic. Nevertheless, coarser features such as vasculature may continue to drive the registration, albeit with lower accuracy.

Finally, it is worth noting here one limitation inherent to any multiwavelength psychophysical apparatus: transverse chromatic aberration (TCA). In our system, retinal images are captured using 840 nm light, and these images are used to track retinal motion and generate a prediction on when to deliver a 680 nm stimulus. Although these beams are aligned to the best of our ability as they travel along the optical path of the AOSLO and are corrected for LCA so that they come to a focus in the same plane, chromatic dispersion within the eye may cause the red stimulus to shift laterally relative to the infrared imaging light source. In the AOSLO, it is possible to estimate TCA offline by comparing images collected simultaneously using red and IR light; however, real-time methods of TCA correction have yet to be developed. The largest TCA we have observed using our system measures about 1.7 arc min when the imaging beam is displaced eccentrically toward the pupil border, where the effect of TCA is most dramatic.[38] Because high-fidelity AOSLO imaging requires good beam centration, TCA values under normal testing conditions are expected to be in the order of 0.7 arc min or less.[39]

Establishing Structure-Function Relationships on the Cellular Scale

AOSLO and other AO-based systems have been used to establish structure-function relationships in the normal human retina.[40,41] Of the studies using AO imaging to obtain structural measures in patients with retinal disorders, only one endeavored to test visual function on a scale commensurate to the imaging.[42] Using 0.75′ AO-corrected stimuli, Makous et al. were able to confirm the presence of microscotomas in the retina of a patient with a disrupted cone mosaic secondary to a middle-wavelength-sensitive cone mutation. Despite an estimated 30% loss of cone photoreceptors, this patient with dichromacy had normal visual
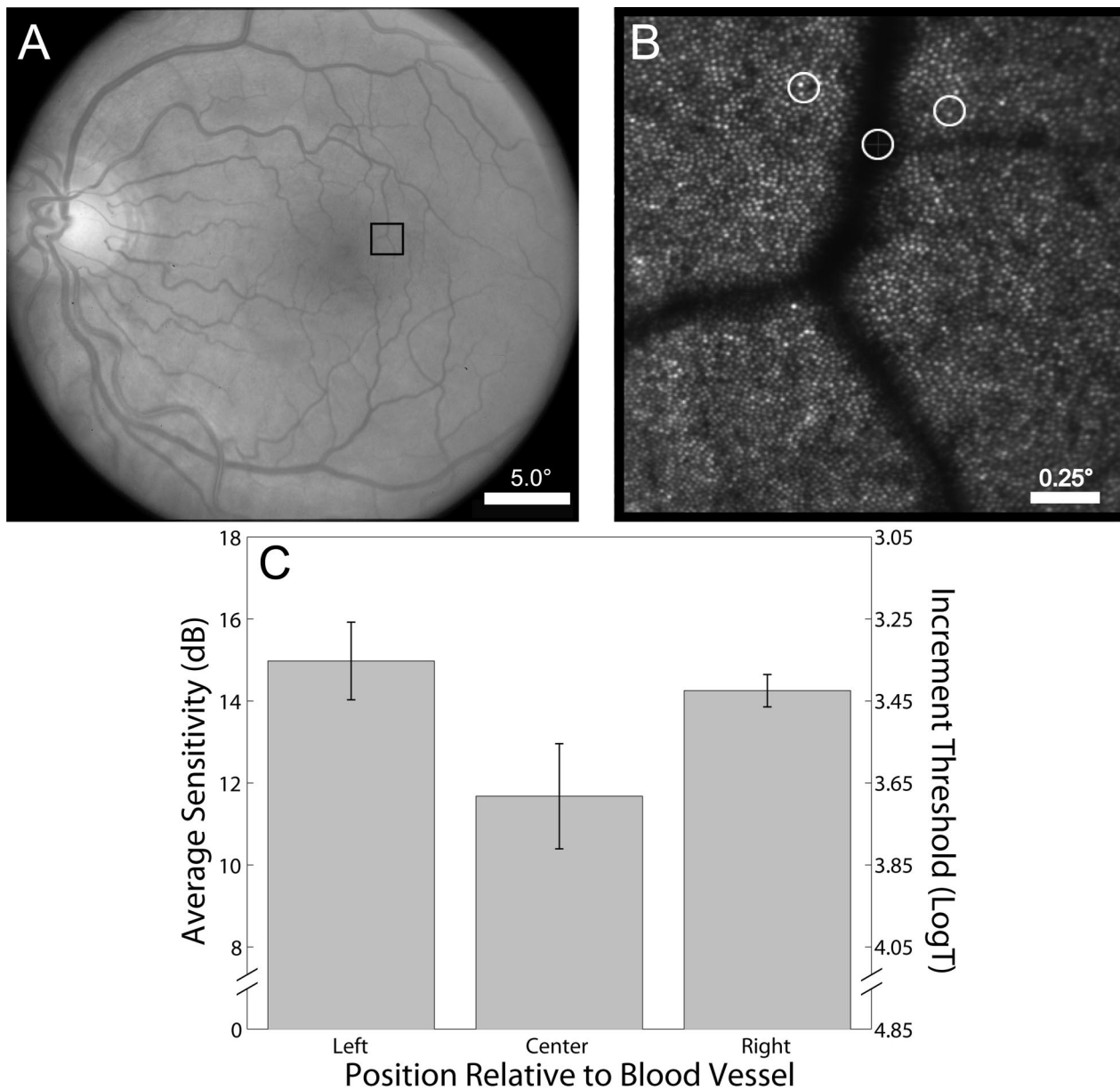
FIGURE 5.

Results from sensitivity testing on and around a parafoveal blood vessel. (A) Fundus photograph with box indicating the blood vessel targeted for AOSLO-based microperimetry (eccentricity ~2.5°). (B) AOSLO image with perimetry test locations indicated. (C) Average sensitivity plotted as a function of stimulus location. (Note: The size of the white circles marking test location represents the size of the test stimulus on the retina.)

acuity and visual field (Humphrey 10-2; stimulus size: Goldmann III) results, suggesting that small spot perimetry may be necessary to establish the functional implications of subtle changes in the photoreceptor mosaic. Other studies also hint at the benefit of using small, non-redundant stimuli—which AO-based systems are ideally suited to generate—to more fully reveal the functional consequences of degenerate photoreceptor arrays.[43,44]

Although the AO microflash method of Makous et al. produced convincing results, it is perhaps too inefficient to be suited for use in the wider patient population. Using a flood-illuminated AO system leaves the examiner unable to target specific regions in the cone mosaic for functional testing. In patients with diffuse photoreceptor loss, this limitation can be overcome by clever experimental design and statistical inference, but measuring visual sensitivity at focal retinal loci—such as a patch of cones at the edge of geographic atrophy in age-related macular degeneration or within a small ROI in a patient with inherited retinal degeneration—with confidence and efficiency would remain a challenge.

The angioscotoma data shown in Fig. 5C serve as a proof-of-concept for using the methods outlined in this article to test focal vision loss. That the blood vessels in the retina cast a shadow on the underlying photoreceptors is not surprising: Purkinje first noted the phenomenon nearly 200 years ago.[45] However, under normal conditions, these shadows are not perceived. It has been postulated that the underlying photoreceptors simply increase their gain to compensate for the decrease in light impinging on them.[45] It is known that the visual system can undergo rapid local adaptation—entoptic images of the retinal vasculature induced by transscleral
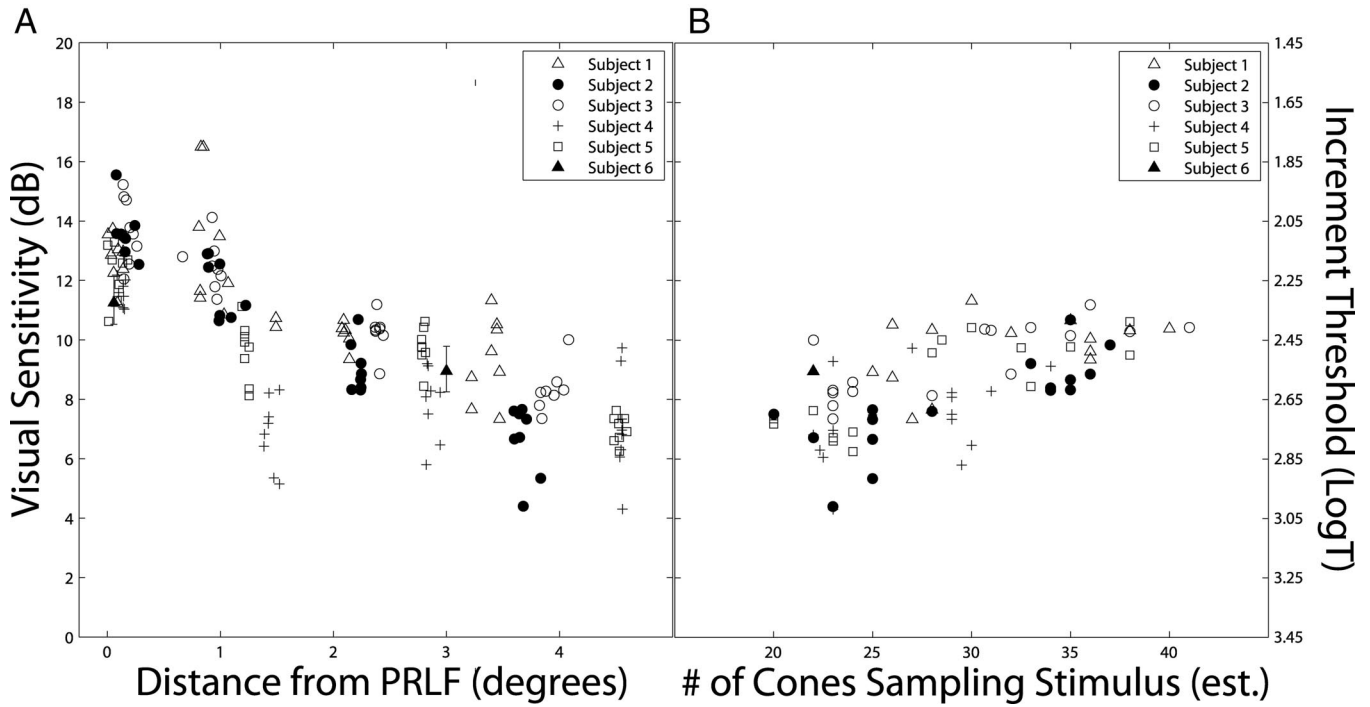
FIGURE 6.

Visual sensitivity as a function of retinal eccentricity and number of cones stimulated. (A) Sensitivity values are plotted in dB as a function of retinal eccentricity, with the corresponding threshold in log Trolands plotted on the secondary y axis. (B) Sensitivity is plotted as a function of the number of cones sampling the stimulus, which is estimated from measures of cone spacing.
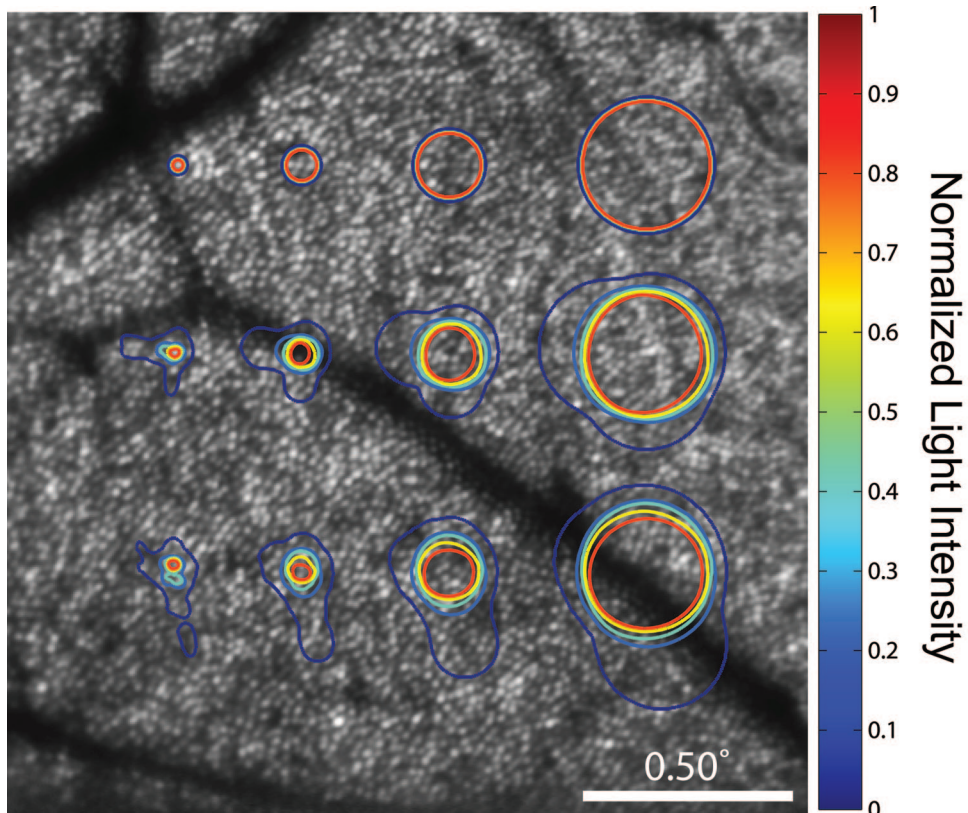
FIGURE 7.

Retinal light distribution of common perimetric stimuli. These distributions, which represent the spread of light on the retina of four perimetric stimuli, were generated by convolution of the stimulus with the point-spread function (PSF) of the diffraction-limited condition (top) and with that of two high-order aberration-uncorrected subjects (middle; bottom). PSFs were calculated for 680 nm light over a 6 mm pupil. Contour lines indicate normalized light intensities for each pixel. The innermost line (red) encircles the photoreceptors which will be stimulated by light at 99% of the intended intensity. Stimuli from left to right: 2.5 arc min circle; Goldman I; Goldmann II; Goldmann III. The retinal eccentricity is approximately 4°.

illumination can fade in as little as 80 ms.[46] This fading is considered analogous to that which occurs when images are stabilized on the retina.[47,48] More recently, it has been observed in some primates that these permanent shadows induce a form of "local amblyopia" on the scale of just a few cones, which is manifested in primary visual cortex of enucleated squirrel monkeys.[49] Although the depth of the defect is contingent on pupil diameter, eye length, and vessel caliber, these results imply that a different, more long-term mechanism may dictate the function of photoreceptors normally falling in the shadow of the blood vessels. Most perimetric studies of angioscotoma are confined to probing function near the large caliber arteries and veins that emerge from the optic disc.[50,51] The data shown in Fig. 5 represent, we believe, the first report of a quantifiable angioscotoma this close to the fovea. While the data in Fig. 5 are preliminary findings, the methods outlined in this report should enable a deeper investigation into how the visual system responds to focal long-term visual deprivation.

To use AOSLO-based microperimetry to establish structure-function relationships in the cone photoreceptor mosaic, it is important to ensure that our measures of visual sensitivity primarily reflect cone function. Rod photoreceptors are effectively blind to the 840 nm background, and they will not be bleached as a result of exposure to it. Furthermore, the absolute spectral sensitivities of the photopic and scotopic visual systems are roughly equivalent at our stimulus wavelength (680 nm).[52] This fact is borne out in the results of Chapanis,[53] who investigated the effect of stimulus wavelength on the dark adaptation curves of normal trichromats and found no rod-cone break when testing with 680 nm light, suggesting that rod contribution to visual sensitivity is equivalent to or less than cone input at this wavelength. As such, it is reasonable to question whether, and to what degree, the measures of visual sensitivity we report may be influenced by input from rod photoreceptors.

The ~0.65 log unit increase in visual threshold from 0° to 5° eccentricity shown in Fig. 6A is slightly steeper than the findings of Stiles' testing with a stimulus of similar wavelength and size.[54] In that study, an increase in increment threshold of roughly 0.6 log units between 0° to 5° eccentricity was found in dark-adapted subjects when testing with a 10 arc min, 700 nm stimulus. For the measures reported here, the subjects were not dark-adapted, and the AOM leak associated with the 680 nm test stimulus produced an equivalent background luminance of 0.70 cd/m², which falls within the mesopic light range. Given that the density of rod photoreceptors increases with eccentricity until about 18° from the fovea,[32] their relative contribution to the overall visual response to 680 nm light is expected to increase with eccentricity. Therefore, one might interpret the steeper drop off in sensitivity in our data as the result of a dampened rod response induced by the mesopic test conditions. At any rate, introducing an external monitor to display an adapting field of sufficient luminance—100 scotopic Trolands[55]—to the subject through a dichroic prism will be implemented for future studies, as it would ensure testing in the photopic regime.

While the visual thresholds shown in Fig. 6A increase with retinal eccentricity in the expected fashion, the data are noisy, and the source of this noise is unclear. For any perimeter, it is essential that variability—both within and between measurement sessions—be assessed thoroughly so that the examiner knows what magnitude of change in sensitivity may be deemed significant. One source of

variability in the sensitivity data reported here is common to all perimeters: stimulus size. In standard automated perimetry, variability in measured thresholds increases as the perimetric stimulus size decreases.[56,57] Normal variability in standard automated perimetry using Goldmann-I stimuli is in the order of °3.5 dB (=0.35 log units), which seems to agree qualitatively with the data presented in 6A, although differences in the testing parameters—including background luminance, test wavelength, and modulation range—of different perimetry devices precludes us from making a direct comparison.

A second potential source of noise may complicate matters further: test wavelength. Normal human color vision is subserved by three classes of photoreceptors: short-, medium-, and long-wavelength sensitive cones (S, M, and L, respectively). The ratio of L and M cones has been shown to vary widely in normal subjects with putatively normal color vision, and random mosaics can give rise to large patches of single cone types.[2,3,58]

For technical reasons, our AOSLO system uses 680 nm light for stimulation. In primates, the absolute sensitivity of L cones to 680 nm light is 14 times greater than that of M cones and 106 times greater than S cones.[59] Because the majority of our data were collected at manually selected test locations for each trial, some of the noise seen in the data in Fig. 6A might be attributed to variations in the L-M ratio in the groups of cones recruited by our Goldmann-I sized stimulus as the test location varied slightly between measurements at a given eccentricity. However, relative adaptation to the imaging laser may serve to mitigate this discrepancy in L and M cone absolute sensitivities. For 840 nm light, L cones are roughly an order of magnitude more sensitive than M cones[60] and thus may exist in a relatively more adapted state during testing. Ultimately, a blue-green adapting background—to which M cones are more sensitive—of the appropriate intensity could be used to counterbalance the relative adaptation induced by the imaging raster. For our purposes, the contribution of S cones, which are relatively rare and evenly distributed, can be ignored.[61]

Ultimately, any potentially negative effects of the discrepancy in L and M cone spectral sensitivities may be largely eliminated by choosing a test wavelength at which they are equally sensitive: 550 nm.[62] Testing sensitivity with 550 nm light under conditions in which the L and M cones are equally adapted may yield less noisy measures of visual sensitivity, but it is not without consequence: (1) because retinal imaging will continue to be conducted with IR light, the effect of TCA will become more pronounced,[13,38] and real-time TCA compensation may have to be implemented to ensure the stimulus is delivered to its target; and (2) owing to the increased sensitivity of rod photoreceptors at shorter wavelengths[52] and the relative adaptation induced by the imaging raster, adapting fields of the appropriate wavelength and luminance will have to be employed.

Finally, the data shown in Fig. 6B highlight the type of analysis possible with AOSLO-based microperimetry. It is clear from Fig. 6B that, under the current test conditions, visual sensitivity is not simply a function of the number of cones sampling the stimulus. If collecting measures of visual sensitivity with 550 nm light and the appropriate adapting background prove less noisy, it may be possible to generate a predictive model of detection that incorporates the number of cone photoreceptors engaged by the stimulus, along with other factors such as photoreceptor aperture, outer segment

length, and ganglion cell pooling.[63] Such a model—which, unlike previous efforts, would not rely entirely on normative optical and anatomical data from the literature—could be useful in analyzing patients with photoreceptor degenerations, allowing the examiner to distinguish between patients whose remaining cones are dysfunctional and those whose remaining cones, although reduced in number, are still functionally normal.

SUPPLEMENTAL DIGITAL CONTENT

Video that demonstrates targeted stimulus delivery in AOSLO-based microperimetry is available online at http://links.lww.com/OPX/A84. In this video, the retinal locus targeted for sensitivity testing is tracked as the eye moves normally during fixation. The white cross written onto the video marks the location of stimulus delivery. The Goldmann I-sized red circle is added during postprocessing to enhance the visualization of the stimulus extent. The field of view is 2.1° × 2.1°.

ACKNOWLEDGMENTS

REFERENCES

1. Liang J, Williams DR, Miller DT. Supernormal vision and high-resolution retinal imaging through adaptive optics. J Opt Soc Am (A) 1997;14:2884–92.

2. Brainard DH, Roorda A, Yamauchi Y, Calderone JB, Metha A, Neitz M, Neitz J, Williams DR, Jacobs GH. Functional consequences of the relative numbers of L and M cones. J Opt Soc Am (A) 2000;17:607–14.

3. Roorda A, Williams DR. The arrangement of the three cone classes in the living human eye. Nature 1999;397:520–2.

4. Roorda A, Romero-Borja F, Donnelly W, III, Queener H, Hebert T, Campbell M. Adaptive optics scanning laser ophthalmoscopy. Opt Express 2002;10:405–12.

5. Duncan JL, Ratnam K, Birch DG, Sundquist SM, Lucero AS, Zhang Y, Meltzer M, Smaoui N, Roorda A. Abnormal cone structure in foveal schisis cavities in X-linked retinoschisis from mutations in exon 6 of the RS1 gene. Invest Ophthalmol Vis Sci 2011;52:9614–23.

6. Duncan JL, Zhang Y, Gandhi J, Nakanishi C, Othman M, Branham KE, Swaroop A, Roorda A. High-resolution imaging with adaptive optics in patients with inherited retinal degeneration. Invest Ophthalmol Vis Sci 2007;48:3283–91.

7. McAllister JT, Dubis AM, Tait DM, Ostler S, Rha J, Stepien KE, Summers CG, Carroll J. Arrested development: high-resolution imaging of foveal morphology in albinism. Vision Res 2010;50:810–7.

8. Talcott KE, Ratnam K, Sundquist SM, Lucero AS, Lujan BJ, Tao W, Porco TC, Roorda A, Duncan JL. Longitudinal study of cone photoreceptors during retinal degeneration and in response to ciliary neurotrophic factor treatment. Invest Ophthalmol Vis Sci 2011;52:2219–26.

9. Wolfing JI, Chung M, Carroll J, Roorda A, Williams DR. High-resolution retinal imaging of cone-rod dystrophy. Ophthalmology 2006;113:1019.e1.

10. Yoon MK, Roorda A, Zhang Y, Nakanishi C, Wong LJ, Zhang Q, Gillum L, Green A, Duncan JL. Adaptive optics scanning laser ophthalmoscopy images in a family with the mitochondrial DNA T8993C mutation. Invest Ophthalmol Vis Sci 2009;50:1838–47.

11. Dubra A, Sulai Y, Norris JL, Cooper RF, Dubis AM, Williams DR, Carroll J. Noninvasive imaging of the human rod photoreceptor mosaic using a confocal adaptive optics scanning ophthalmoscope. Biomed Opt Express 2011;2:1864–76.

12. Merino D, Duncan JL, Tiruveedhula P, Roorda A. Observation of cone and rod photoreceptors in normal subjects and patients using a new generation adaptive optics scanning laser ophthalmoscope. Biomed Opt Express 2011;2:2189–201.

13. Dubra A, Sulai Y. Reflective afocal broadband adaptive optics scanning ophthalmoscope. Biomed Opt Express 2011;2:1757–68.

14. Okada K, Yamamoto S, Mizunoya S, Hoshino A, Arai M, Takatsuna Y. Correlation of retinal sensitivity measured with fundus-related microperimetry to visual acuity and retinal thickness in eyes with diabetic macular edema. Eye (Lond) 2006;20:805–9.

15. Schmitz-Valckenberg S, Bultmann S, Dreyhaupt J, Bindewald A, Holz FG, Rohrschneider K. Fundus autofluorescence and fundus perimetry in the junctional zone of geographic atrophy in patients with age-related macular degeneration. Invest Ophthalmol Vis Sci 2004;45:4470–6.

16. Sjaarda RN, Frank DA, Glaser BM, Thompson JT, Murphy RP. Assessment of vision in idiopathic macular holes with macular microperimetry using the scanning laser ophthalmoscope. Ophthalmology 1993;100:1513–8.

17. Takamine Y, Shiraki K, Moriwaki M, Yasunari T, Miki T. Retinal sensitivity measurement over drusen using scanning laser ophthalmoscope microperimetry. Graefes Arch Clin Exp Ophthalmol 1998;236:285–90.

18. Midena E, Vujosevic S, Cavarzeran F. Normal values for fundus perimetry with the microperimeter MP1. Ophthalmology 2010;117:1571–6.

19. Sunness JS, Schuchard RA, Shen N, Rubin GS, Dagnelie G, Haselwood DM. Landmark-driven fundus perimetry using the scanning laser ophthalmoscope. Invest Ophthalmol Vis Sci 1995;36:1863–74.

20. Midena E, ed. Perimetry and the Fundus: An Introduction to Microperimetry. Thorofare, NJ: SLACK Inc.; 2007.

21. Enoch JM, Le DA. Comparison of the Canon CPP-1 and the new Nidek MP-1 45 degree fundus camera perimeters: studies around and on top of the optic nerve head in myopia. Invest Ophthalmol Vis Sci 2004;45:E-Abstract 2772.

22. Woods RL, Vera-Diaz FA, Lichtenstein L, Peli E. Spatial alignment of microperimeters. Invest Ophthalmol Vis Sci 2007;48:E-Abstract 144.

23. Arathorn DW, Yang Q, Vogel CR, Zhang Y, Tiruveedhula P, Roorda A. Retinally stabilized cone-targeted stimulus delivery. Opt Express 2007;15:13731–44.

24. Yang Q, Arathorn DW, Tiruveedhula P, Vogel CR, Roorda A. Design of an integrated hardware interface for AOSLO image capture and cone-targeted stimulus delivery. Opt Express 2010;18:17841–58.

25. Sincich LC, Zhang Y, Tiruveedhula P, Horton JC, Roorda A. Resolving single cone inputs to visual receptive fields. Nat Neurosci 2009;12:967–9.

26. Grieve K, Tiruveedhula P, Zhang Y, Roorda A. Multi-wavelength imaging with the adaptive optics scanning laser Ophthalmoscope. Opt Express 2006;14:12230–42.

27. Rossi EA, Roorda A. Is visual resolution after adaptive optics correction susceptible to perceptual learning? J Vis 2010;10:11.

28. Rossi EA, Weiser P, Tarrant J, Roorda A. Visual performance in emmetropia and low myopia after correction of high-order aberrations. J Vis 2007;7:14.

29. Poonja S, Patel S, Henry L, Roorda A. Dynamic visual stimulus presentation in an adaptive optics scanning laser ophthalmoscope. J Refract Surg 2005;21:S575–80.

30. Watson AB, Pelli DG. QUEST: a Bayesian adaptive psychometric method. Percept Psychophys 1983;33:113–20.

31. Li KY, Roorda A. Automated identification of cone photoreceptors in adaptive optics retinal images. J Opt Soc Am (A) 2007;24:1358–63.

32. Curcio CA, Sloan KR, Kalina RE, Hendrickson AE. Human photoreceptor topography. J Comp Neurol 1990;292:497–523.

33. Atchison DA, Smith G. Chromatic dispersions of the ocular media of human eyes. J Opt Soc Am (A) 2005;22:29–37.

34. Guizar-Sicairos M, Thurman ST, Fienup JR. Efficient subpixel image registration algorithms. Opt Lett 2008;33:156–8.

35. Evans JN. A contribution to the study of angioscotometry. Br J Ophthalmol 1927;11:369–84.

36. Bedggood P, Daaboul M, Ashman R, Smith G, Metha A. Characteristics of the human isoplanatic patch and implications for adaptive optics retinal imaging. J Biomed Opt 2008;13:024008.

37. Pallikaris A, Williams DR, Hofer H. The reflectance of single cones in the living human eye. Invest Ophthalmol Vis Sci 2003;44:4580–92.

38. Thibos LN, Bradley A, Still DL, Zhang X, Howarth PA. Theory and measurement of ocular chromatic aberration. Vision Res 1990;30:33–49.

39. Harmening WM, Roorda A. Objective measurement of transverse chromatic aberration with the adaptive optics scanning laser ophthalmoscope. Abstract presented at the Optical Society of America—Fall Vision Meeting, September 2011, Seattle, WA. Available at: http://w.journalofvision.org/content/11/15/42.abstract?sid=80309aab-6012-4067-a235-e14b2143a824. Accessed February 9, 2012.

40. Hofer H, Singer B, Williams DR. Different sensations from cones with the same photopigment. J Vis 2005;5:444–54.

41. Rossi EA, Roorda A. The relationship between visual resolution and cone spacing in the human fovea. Nat Neurosci 2010;13:156–7.

42. Makous W, Carroll J, Wolfing JI, Lin J, Christie N, Williams DR. Retinal microscotomas revealed with adaptive-optics microflashes. Invest Ophthalmol Vis Sci 2006;47:4160–7.

43. Geller AM, Sieving PA. Assessment of foveal cone photoreceptors in Stargardt's macular dystrophy using a small dot detection task. Vision Res 1993;33:1509–24.

44. Geller AM, Sieving PA, Green DG. Effect on grating identification of sampling with degenerate arrays. J Opt Soc Am (A) 1992;9:472–7.

45. Westheimer G. Entoptic phenomena. In: Kaufman PL, Alm A, Adler FH, eds. Adler's Physiology of the Eye: Clinical Application, 10th ed. St. Louis, MO: Mosby; 2003:441–52.

46. Coppola D, Purves D. The extraordinarily rapid disappearance of entopic images. Proc Natl Acad Sci USA 1996;93:8001–4.

47. Ditchburn RW, Ginsborg BL. Vision with a stabilized retinal image. Nature 1952;170:36–7.

48. Riggs LA, Ratliff F, Cornsweet JC, Cornsweet TN. The disappearance of steadily fixated visual test objects. J Opt Soc Am 1953;43:495–501.

49. Adams DL, Horton JC. Shadows cast by retinal blood vessels mapped in primary visual cortex. Science 2002;298:572–6.

50. Remky A, Beausencourt E, Elsner AE. Angioscotometry with the scanning laser ophthalmoscope. Comparison of the effect of different wavelengths. Invest Ophthalmol Vis Sci 1996;37:2350–5.

51. Schiefer U, Benda N, Dietrich TJ, Selig B, Hofmann C, Schiller J. Angioscotoma detection with fundus-oriented perimetry. A study with dark and bright stimuli of different sizes. Vision Res 1999;39:1897–909.

52. Wald G. Human vision and the spectrum. Science 1945;101:653–8.

53. Chapanis A. The dark adaptation of the color anomalous measured with lights of different hues. J Gen Physiol 1947;30:423–37.

54. Stiles WS. Increment thresholds and the mechanisms of colour vision. Doc Ophthalmol 1949;3:138–65.

55. Aguilar M, Stiles WS. Saturation of the rod mechanism of the retina at high levels of stimulation. Optica Acta 1954;1:59–65.

56. Gilpin LB, Stewart WC, Hunt HH, Broom CD. Threshold variability using different Goldmann stimulus sizes. Acta Ophthalmol (Copenh) 1990;68:674–6.

57. Vislisel JM, Doyle CK, Johnson CA, Wall M. Variability of rarebit and standard perimetry sizes I and III in normals. Optom Vis Sci 2011;88:635–9.

58. Hofer H, Carroll J, Neitz J, Neitz M, Williams DR. Organization of the human trichromatic cone mosaic. J Neurosci 2005;25:9669–79.

59. Baylor DA, Nunn BJ, Schnapf JL. Spectral sensitivity of cones of the monkey *Macaca fascicularis*. J Physiol 1987;390:145–60.

60. Wyszecki GN, Stiles WS. Color Science: Concepts and Methods, Quantitative Data and Formulae, 2nd ed. New York, NY: Wiley; 1982.

61. Curcio CA, Allen KA, Sloan KR, Lerea CL, Hurley JB, Klock IB, Milam AH. Distribution and morphology of human cone photoreceptors stained with anti-blue opsin. J Comp Neurol 1991;312:610–24.

62. Wald G. The receptors of human color vision. Science 1964;145:1007–16.

63. Banks MS, Sekuler AB, Anderson SJ. Peripheral spatial vision: limits imposed by optics, photoreceptors, and receptor pooling. J Opt Soc Am (A) 1991;8:1775–87.

William S. Tuten
University of California
485 Minor Hall
Berkeley, California 94720-2020
e-mail: wtuten@berkeley.edu